

360° High-Resolution Depth Estimation via Uncertainty-aware Structural Knowledge Transfer

Zidong Cao, Hao Ai, Athanasios V. Vasilakos, *IEEE Senior Member*, Lin Wang[†], *Member, IEEE*

Abstract—To predict high-resolution (HR) omnidirectional depth map, existing methods typically leverage HR omnidirectional image (ODI) as the input via fully-supervised learning. However, in practice, taking HR ODI as input is undesired due to resource-constrained devices. In addition, depth maps are often with lower resolution than color images. Therefore, in this paper, we explore for the first time to estimate the HR omnidirectional depth directly from a low-resolution (LR) ODI, when no HR depth GT map is available. Our key idea is to transfer the scene structural knowledge from the HR image modality and the corresponding LR depth maps to achieve the goal of HR depth estimation without any extra inference cost. Specifically, we introduce ODI super-resolution (SR) as an auxiliary task and train both tasks collaboratively in a weakly supervised manner to boost the performance of HR depth estimation. The ODI SR task extracts the scene structural knowledge via uncertainty estimation. Buttressed by this, a scene structural knowledge transfer (SSKT) module is proposed with two key components. First, we employ a cylindrical implicit interpolation function (CIIF) to learn cylindrical neural interpolation weights for feature up-sampling and share the parameters of CIIFs between the two tasks. Then, we propose a feature distillation (FD) loss that provides extra structural regularization to help the HR depth estimation task learn more scene structural knowledge. Extensive experiments demonstrate that our weakly-supervised method outperforms baseline methods, and even achieves comparable performance with the fully-supervised methods.

Impact Statement—Our weakly-supervised can adapt to various backbones, input sizes, and datasets. Our method can also easily be applied to higher resolution, such as 1024×2048 . We contribute the effectiveness to the proposed SSKT module, which successfully transfers essential scene structural knowledge from the ODI SR task to HR depth estimation task. Importantly, we prove that the way of transferring the scene structural knowledge from the HR image modality and corresponding LR depth map is feasible to achieve the goal of HR depth estimation without any extra inference cost.

Index Terms—Omnidirectional image, depth estimation, image super-resolution, knowledge transfer, weakly-supervised learning

I. INTRODUCTION

Monocular depth estimation is a fundamental task of 3D scene understanding that finds its applications in various fields, such as autonomous driving. The advancements in deep

Z. Cao, H. Ai are with the Artificial Intelligence Thrust, The Hong Kong University of Science and Technology (HKUST), Guangzhou, China. E-mail: {caozidong1996@gmail.com, hai033@connect.hkust-gz.edu.cn}

Athanasios V. Vasilakos is with the Center for AI Research (CAIR), University of Agder(UiA), Grimstad, Norway. Email: thanos.vasilakos@uia.no

L. Wang is with the Artificial Intelligence Thrust, HKUST, Guangzhou, and Dept. of Computer Science and Engineering, HKUST, Hong Kong SAR, China. E-mail: linwang@ust.hk.

[†]Corresponding author

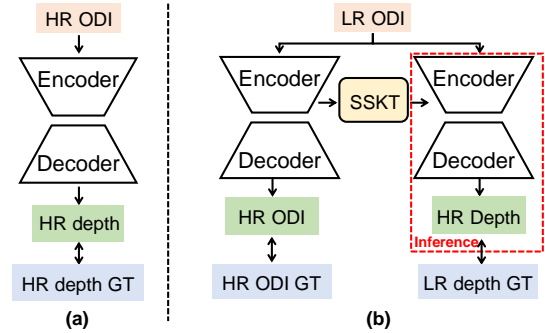


Fig. 1. HR depth estimation paradigms. (a) Existing fully-supervised methods. (b) Our weakly-supervised method transfers knowledge between two tasks via the SSKT module.

neural networks (DNNs) [1] and the accessibility of large-scale annotated datasets have resulted in notable improvements in monocular depth estimation. Nevertheless, most of the existing approaches are developed for perspective images, which suffer from a limited field-of-view (FoV) [2]–[8].

Recently, 360° cameras¹ have received considerable attention because of their ability to capture the environment with a wide FoV of $180^\circ \times 360^\circ$ in a single shot. Omnidirectional images (ODIs)² present the scene entirely with rich scene contexts. This distinct advantage has inspired active research for monocular depth estimation [9]–[12]. However, the angular resolution of ODIs is relatively lower than that of perspective images when ODIs and perspective images are captured by different sensors with the identical size. The low angular resolution leads to degraded structural details such as edges, rendering it difficult for omnidirectional depth estimation.

To reconstruct the structural details, existing methods [10]–[18] leverage high-resolution (HR) ODIs as inputs with the supervision of HR depth ground truth (GT) maps. For instance, using the HR ODIs and paired HR depth GT maps, OmniDepth [14] employs the encoder-decoder architecture to predict HR depth maps, as shown in Fig. 1(a). However, in practice, taking HR ODI as input is undesired by resource-constrained devices. Take virtual reality (VR) as an example, the headsets often have limited bandwidth for transmission and limited computational resources [19], [20]. Processing HR ODIs in the headsets might cause high latency due to limited bandwidth [19]. In addition, obtaining HR depth maps is arduous and expensive [21]. This is because depth sensors, such as LiDARs, often capture sparse depths with low resolution [22]. Also, increasing the lens of LiDARs is

¹Also called omnidirectional cameras.

²ODIs usually indicate the equirectangular projection (ERP) type images.

far more expensive than obtaining HR ODI [23].

Motivation. In this paper, we explore for the first time to estimate the HR depth map directly from an LR ODI, when no HR depth GT map is available (See Fig 1(b)). Without the supervision of HR depth GT maps, the fine scene structural details can scarcely be recovered in the HR depth predictions. Therefore, to explore valuable supplementary supervision that can facilitate HR depth estimation, our key idea is to learn and transfer scene structural knowledge from the HR image modality and the corresponding LR depth maps to achieve the goal of HR depth estimation without causing extra inference cost. This is inspired by the fact that **1**) there exist publicly available large-scale LR-HR paired ODIdataset and thus achieve the ODI super-resolution (SR) task [24], [25]; **2**) an ODI and its corresponding depth map are photometric and geometric representations of the same scene, respectively [21]. This implies that both representations share the common scene structural knowledge, such as edges [26].

Specifically, we employ the ODI SR as an auxiliary task and train both tasks collaboratively in a weakly-supervised manner to boost the performance of HR depth estimation. The ODI SR task takes an LR ODI as input to predict a super-resolved RGB image. As the textural details in the super-resolved RGB image may interfere with the smoothness of depth prediction [10], [27], we introduce uncertainty estimation [28] for the ODI SR task to specially extract the scene structural knowledge. The high-uncertainty regions are often matched with high-frequency regions, which can be utilized to emphasize the regions carrying more structural knowledge [28]. Upon this, we propose a scene structural knowledge transfer (SSKT) module with two key components.

Firstly, considering the unique properties of the equirectangular projection (ERP) type of ODIs, we design a novel cylindrical implicit interpolation function (CIIF) for feature up-sampling by learning the neural interpolation weights based on cylindrical coordinates. This way, our CIIF alleviates the discontinuity and stretched distortion of ODIs. Also, as the learned interpolation weights can capture the correlations among neighboring pixels, they can be used to represent the scene structural knowledge. Therefore, by sharing the parameters of CIIFs between the ODI SR and HR depth estimation tasks, structural knowledge can be transferred between the two tasks effectively. Secondly, as the features of the ODI SR task also contain crucial scene structural knowledge, we propose a feature distillation (FD) loss to further boost the HR depth estimation performance.

In total, our weakly-supervised method is *efficient*, as the ODI SR network and SSKT module can be removed freely and only LR ODI is needed during inference, introducing no extra inference cost. Moreover, our method is *flexible* and can be easily adapted as a plug-and-play approach by modifying the backbones for the HR depth estimation network and varying the up-sampling factors (See Tab. I). Furthermore, we demonstrate the *effectiveness* of our method across different datasets, [14], [29], [30], with various up-sampling factors and backbones. The experimental results show that our method not only *outperforms* the baseline methods, but also achieves *comparable* performance with the fully-supervised methods.

Our main contributions can be summarized into four-fold:

- We propose the first weakly-supervised method that predicts the HR omnidirectional depth map from an LR ODI, when no HR depth GT map is available.
- We propose to learn and transfer the scene structural knowledge from an uncertainty-driven ODI SR task.
- We propose an SSKT module with two components. The first is the CIIF as it is specific for ODIs to learn neural interpolation weights, whose parameters are shared between the two tasks. The second is the FD loss to provide extra structural regularization.
- Experimental results demonstrate that our weakly supervised method is efficient, flexible, and effective, which can achieve comparable results with the fully supervised methods.

II. RELATED WORK

Omnidirectional Monocular Depth Estimation. Some attempts have been made to tackle the spherical distortion in ODIs by modifying the characteristics of convolutional filters, including row-wise rectangular filter [14], deforming the sampling grids [16], and dilated convolutions for larger receptive fields [17]. Another direction is to combine different projection types, *e.g.*, ERP, cube map [10], [12], and tangent projection [13], [31]. BiFuse [12] proposes a bi-projection fusion model for the ERP images and cube maps to share information between each other, while UniFuse [10] demonstrates that the unidirectional fusion from the cube map to ERP is more effective. Some methods [15], [18] focus on parallel computation in omnidirectional monocular depth estimation. The typical pipeline is first projecting an ERP image into multiple low-resolution perspective patches, then predicting depth maps in parallel, and finally re-projecting the perspective depth predictions back to the ERP plane. Recently, Li *et al.* [32] propose to extract features on the unit sphere to relieve the distortion effect. However, all the aforementioned methods require the HR depth maps for supervision.

Omnidirectional image super-resolution. Early ODI SR methods [33]–[35] assemble multiple LR ODIs to reconstruct an HR one. However, they rely heavily on the precision of calibration and the number of inputs. Cagri *et al.* [36] propose the first DNN-based framework via adversarial learning. LAU-Net [24] addresses the non-uniformly distributed pixel density of the ERP type ODI via adaptively up-sampling different latitude bands. SphereSR [25] proposes a continuous spherical representation to model the spherical data as an icosahedron and reconstruct ODIs with multiple projection types. Recently, OSRT [37] and OPDN [38] employ distortion-aware transformers to alleviate the effect of distortion in ERP type ODI.

Modeling Uncertainty in image super-resolution. In the image SR task, high-frequency regions with rich texture and edges carry more visual information than the smooth regions [28]. To better capture the high-frequency details and emphasize the corresponding pixels, some uncertainty-driven image SR methods have been proposed [28], [39]. For instance, GRAM [39] extracts the uncertainty map via the Gaussian assumption and takes the uncertainty map as

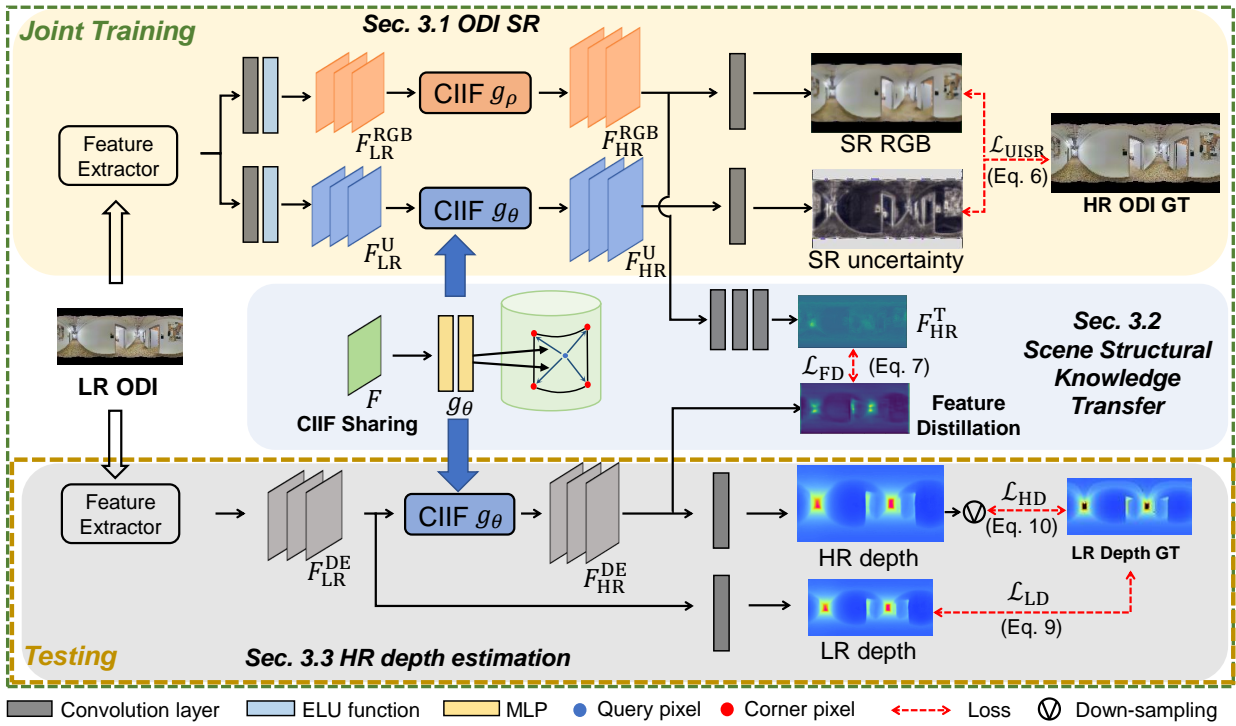


Fig. 2. **Overview of our weakly-supervised framework.** Firstly, we introduce an ODI SR task (Sec III-A) which predicts uncertainty to extract structural knowledge. Then, we design an SSKT module with CIIF that learns cylindrical neural interpolation weights and shares parameters between the two tasks. The SSKT module also includes an FD loss (Sec III-B) for feature distillation. Finally, we employ an HR depth estimation task (Sec III-C) to generate HR depth estimation directly from an LR ODI. The detailed components of CIIF is shown in Fig. 3(b).

the attenuation mask to achieve better performance. Differently, Ning *et al.* [28] estimate the uncertainty with Jeffrey’s prior [40] and proposes an uncertainty-driven loss to provide the attention for the pixels with high uncertainty. Our method introduces the uncertainty estimation to extract scene structural knowledge, which is transferred to depth estimation task.

Implicit Neural Representation. It uses few parameters with the help of multi-layer perceptrons (MLPs) [41]–[43]. For the image SR task, Chen *et al.* [44] propose an implicit function, LIIF, to represent images continuously and achieves the up-sampling process with arbitrary factor. Furthermore, Tang *et al.* [45] replace the non-parametric interpolation weights in LIIF with the ones learned from the input image and depth map to achieve the guided depth SR task. However, the two mentioned implicit functions are based on the Cartesian coordinate system, which is weak in tackling the discontinuity and distortion problems in the ERP type ODIs. In contrast, our proposed cylindrical implicit interpolation function (CIIF) is constructed based on cylindrical coordinates, which is effective to alleviate the mentioned problems in ERP type ODIs.

Multi-task learning. It is mainly used for correlated tasks [46], *e.g.*, semantic segmentation and depth estimation [47]. Liu *et al.* [48] leverage 3D features to enhance 2D features extracted from the images. Wang *et al.* [49] treat image SR as an auxiliary task for semantic segmentation with fully supervision. Sun *et al.* [21] leverage the monocular depth estimation task to facilitate the depth SR task, reconstructing finer the structural details. In addition, Yang *et al.* [50] proposes a cross-domain attention conciliation module to enhance the depth feature when encoding the image and depth

features. Different from these methods, based on the geometric similarity, we aim to transfer structural knowledge from the fully-supervised ODI SR task to the weakly-supervised HR depth estimation task.

III. METHOD

Overview. The goal is to predict an HR omnidirectional depth map D_{HR} from an LR ODI I_{LR} as input, using only an LR depth map D_{LR}^{GT} for supervision. As shown in Fig. 2, our framework consists of an ODI SR task, a scene structural knowledge transfer (SSKT) module, and an HR depth estimation task. The ODI SR is employed as an auxiliary task and trained collaboratively with the HR depth estimation task. Specifically, we introduce uncertainty estimation to the ODI SR task for scene structural knowledge extraction. To transfer the extracted knowledge, the SSKT module is proposed with two components. The first is to share the parameters of the proposed cylindrical implicit interpolation function (CIIF) between the two tasks. The second is the feature distillation (FD) loss that provides extra structural regularization. We now describe the components in detail.

A. ODI SR

The omnidirectional images contain not only the complete structural details of the surroundings, but also rich textural details in the scenes. However, the enriched textural details can interfere with the smoothness of predicted depth maps [10], [11], [27]. Therefore, directly transferring knowledge from the ODI SR task degrades the depth estimation performance (See

Tab. III). Inspired by the recent progress of uncertainty-driven image super-resolution [28], which demonstrates that regions with high uncertainty are often matched with high-frequency regions, we introduce the uncertainty estimation to the ODI SR task. By doing so, the regions that carry more structural knowledge can be emphasized, which is beneficial to reconstruct more structural details in the HR depth estimation task. Specifically, as shown in Fig. 2, we utilize the feature extractor to process the LR ODI I_{LR} , and utilize two groups of convolutional layers with ELU activation functions [51] to output LR features for the RGB part F_{LR}^{RGB} and uncertainty part F_{LR}^U , respectively. Then, F_{LR}^{RGB} and F_{LR}^U are up-sampled by CIIFs with parameters g_ρ and g_θ to generate HR features F_{HR}^{RGB} and F_{HR}^U , respectively. We then describe the components of CIIF that achieve the feature up-sampling process.

CIIF. As depicted in Fig. 3(a), the image interpolation problems can be defined as follows:

$$I_{HR}(x_q) = \sum_{i \in N_q} w_{q,i} I_{LR}(x_i), \quad (1)$$

where x_q is the coordinate of query pixel q in the HR image domain, x_i is the coordinate of corner pixel i in the LR image domain; N_q represents the neighboring pixels of q in the LR image domain and $w_{q,i}$ is the interpolation weight between pixel q and i . In LIIF [44], as shown in Fig. 3(a), given the latent code z_i encoded from I_{LR} and the coordinate relation between q and i , the RGB value of q in the HR image domain is predicted by the MLP f_θ with parameters θ as follows:

$$I_{HR}(x_q) = f_\theta(z_i, x_q - x_i). \quad (2)$$

To address the border discontinuity issue, LIIF [44] averages the four predictions of query pixel q from its four corner pixels. Notably, the interpolation weight $w_{q,i}$ is calculated by the partial area S_i diagonally opposite to the corner pixel i (See Fig. 3(a)). Thus, Eq. (2) can be extended to:

$$I_{HR}(x_q) = \sum_{i=1}^4 \frac{S_i}{\sum_{i=1}^4 S_i} f_\theta(z_i, x_q - x_i). \quad (3)$$

Furthermore, [45] replaces the scale factor S_i in Eq. (3) with learnable interpolation weights to obtain smoother results. However, for ODIs with ERP type, which are unfolded from the sphere in a cylindrical manner, there are two specific challenges: 1) The discontinuity between the left and right sides; 2) The stretched distortion toward the poles (the top and bottom of ODIs). Previous implicit interpolation methods, *e.g.* [44], [45], are based on the Cartesian coordinate, which are less effective in representing spatial correlation of pixels in ODIs [25]. Therefore, we propose to reframe ODIs with the cylindrical representation, as shown in Fig. 3(b). The cylindrical angle coordinate is formulated as $\alpha \in (-\arctan(\frac{\pi h}{w}), \arctan(\frac{\pi h}{w}))$ (Latitude angle), $\beta \in (-\pi, \pi)$ (Longitude angle). For the calculation of the cylindrical representation, we recommend readers to refer to the first section of the supplemental material. Based on the cylindrical angle coordinate, we learn the cylindrical implicit interpolation weights (See Fig. 3(b)):

$$w_{q,i} = g_\theta(z_i, (\alpha_i - \alpha_q, \beta_i - \beta_q)). \quad (4)$$

After obtaining the interpolation weights $w_{q,i}$ in Eq. (4),

we combine the weights $w_{q,i}$ with latent code z_i from the LR feature F_{LR} to obtain an HR feature F_{HR} . Finally, the HR features are processed with two different convolutional layers to output the super-resolved RGB image (*i.e.*, mean) μ_{HR} and super-resolved uncertainty map (*i.e.*, variance) σ_{HR} , respectively. Formally, by assuming that uncertainty meets the Laplace distribution, an HR ODI is described as:

$$I_{HR} = \mu_{HR} + \epsilon \times \sigma_{HR}, \quad (5)$$

where ϵ represents the Laplace distribution with the zero mean and unit variance. Specifically, we employ the first stage of [28] with the maximum likelihood estimation (MLE). For stable training, we utilize the logarithmic form of uncertainty $s = \log \sigma_{HR}$. The uncertainty-driven ODI SR loss function \mathcal{L}_{UISR} can be formulated as:

$$\mathcal{L}_{UISR} = \frac{1}{N} \sum_{i=1}^N e^{-s} \left\| I_{HR}^{GT,i} - \mu_{HR}^i \right\|_1 + 2s, \quad (6)$$

where N is the number of pixels, and I_{HR}^{GT} is HR GT image.

B. Scene Structural Knowledge Transfer (SSKT)

After extracting structural knowledge from the ODI SR task, we propose the SSKT module with two components to transfer the extracted knowledge to the HR depth estimation task. Buttressed by the learned interpolation weights of CIIF, we share the parameters g_θ of CIIF between the two tasks. Besides, we propose the feature distillation (FD) loss to further utilize the scene structural knowledge contained in the features of the ODI SR task. The detail of the CIIF sharing strategy and FD loss is introduced in the following part.

CIIF sharing strategy: The CIIF consists of the MLPs and is designed to predict the neural interpolation weights. As the interpolation weights for feature up-sampling can capture the correlations among neighboring pixel features, which can represent the scene structural knowledge. Therefore, it is reasonable to share the parameters g_θ of CIIF between the two tasks for structural knowledge transfer. We do not consider sharing the parameters g_ρ , mainly because it additionally learns textural knowledge that will influence the performance of the HR depth estimation task (See Tab. III). Also, we design to directly share the parameters, instead of asynchronous methods [52] to approximate the parameters of CIIFs. The reason is that the HR depth estimation task is in a weakly-supervised manner, where the structural details are scarcely possible to be recovered, while the ODI SR task can be fully-supervised to provide rich and fine scene structural details (See Tab. IV). Therefore, directly sharing parameters of CIIF between the two tasks is more effective for structural knowledge transfer.

FD Loss: The CIIF sharing strategy can benefit the feature up-sampling process in the HR depth estimation task. To further enhance the structural details in the HR depth prediction, we propose the FD loss as a structural regularization to help two tasks learn common scene structural knowledge. Although ODIs and their corresponding depth maps are two different representations for the same scene with high geometric similarity, simply applying feature similarity loss, *e.g.*, cosine similarity loss, introduces unnecessary textural knowledge and

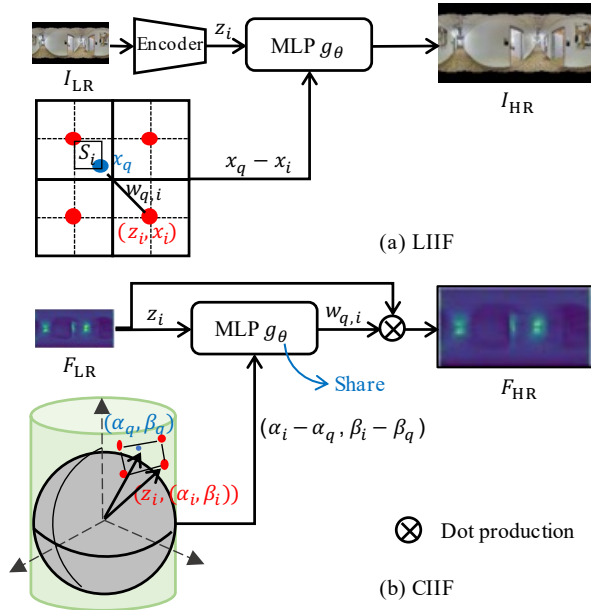


Fig. 3. (a) LIIF predicts the RGB value based on the Cartesian coordinates. (b) Our CIIF learns neural interpolation weights based on the cylindrical coordinates. The parameters of CIIF g_θ are contained in the MLP shared from the ODI SR task.

thus destroys the smoothness of the depth map. To address it, we propose to first transform the HR feature in the RGB part of ODI SR network to simulate the HR feature in the HR depth estimation network. Given an HR feature F_{HR}^{RGB} as input, an encoder consisting of three convolutional layers and ReLU activation functions is applied to obtain a transformed feature F_{HR}^T . We then aim to maximize the cosine similarity between F_{HR}^T and HR feature F_{HR}^{DE} from the HR depth estimation network. FD loss can be formulated as follows:

$$\mathcal{L}_{FD} = 1 - \cos(F_{HR}^T, F_{HR}^{DE}). \quad (7)$$

To supervise the transformed feature F_{HR}^T , we cascade a convolutional layer to process F_{HR}^T and output HR transformed depth map D_{HR}^T . Then we down-sample D_{HR}^T with the max-pooling operation M and supervise it using the LR depth GT map D_{LR}^{GT} with Berhu loss \mathcal{B} [53], formulated as follows:

$$\mathcal{L}_T = \mathcal{B}(M(D_{HR}^T), D_{LR}^{GT}),$$

$$\mathcal{B}(x) = \begin{cases} |x|, & |x| \leq c \\ \frac{x^2 + c^2}{2c}, & |x| > c, \end{cases} \quad (8)$$

where c is a threshold and set to 0.2 empirically [10].

C. HR Depth Estimation

Lastly, the HR depth estimation network leverages the transferred scene structural knowledge to estimate the HR depth map. As shown in Fig. 2, taking an LR ODI I_{LR} as input, the feature extractor outputs an LR feature F_{LR}^{DE} with the same resolution as I_{LR} . Then, the LR feature I_{LR} is processed with two paths. First, I_{LR} is processed with a convolutional layer to output an LR depth prediction D_{LR} , which is directly supervised by D_{LR}^{GT} through Berhu loss \mathcal{B} as follows:

$$\mathcal{L}_{LD} = \mathcal{B}(D_{LR}, D_{LR}^{GT}). \quad (9)$$

Meanwhile, F_{LR}^{DE} is up-sampled with CIIF of shared parameters g_θ , to generate an HR feature F_{HR}^{DE} . F_{HR}^{DE} is then fed into another convolutional layer to predict an HR depth map D_{HR} . We first down-sample D_{HR} with the max-pooling operation M and then apply Berhu loss to supervise it as follows:

$$\mathcal{L}_{HD} = \mathcal{B}(M(D_{HR}), D_{LR}^{GT}). \quad (10)$$

D. Objective Function

The total loss \mathcal{L}_{TOTAL} includes five parts: uncertainty-driven ODI SR loss \mathcal{L}_{UISR} , FD loss \mathcal{L}_{FD} , and three weakly-supervised depth estimation losses: LR depth estimation loss \mathcal{L}_{LD} , HR depth estimation loss \mathcal{L}_{HD} , and transformed depth estimation loss \mathcal{L}_T . \mathcal{L}_{TOTAL} can be formulated as follows:

$$\mathcal{L}_{TOTAL} = \lambda_1 \mathcal{L}_{UISR} + \lambda_2 \mathcal{L}_{FD} + \lambda_3 \mathcal{L}_{LD} + \lambda_4 \mathcal{L}_{HD} + \lambda_5 \mathcal{L}_T, \quad (11)$$

where $\lambda_i, i \in \{1, 2, 3, 4, 5\}$ is a hyper-parameter for i -th loss term in Eq. (11).

IV. EXPERIMENTS

A. Implementation Details

Dataset. We conduct on three datasets: Stanford2D3D [29], Matterport3D [30] and 3D60 [14]. Stanford2D3D and Matterport3D are real-world datasets, and 3D60 is a synthetic dataset, provided by OmniDepth [14]. We follow UniFuse to split the three datasets respectively. The sizes of ODIs and paired depth maps are 512×1024 in Stanford2D3D and Matterport3D, and 256×512 in 3D60. On real-world datasets, the up-sampling factors are set to $\times 4$ and $\times 8$. We test on the synthetic dataset with $\times 8$ up-sampling factor to verify the generalization ability.

Implementation. We use three omnidirectional monocular depth estimation methods as backbones to extract features from the input ODIs: OmniDepth [14] with spherical convolutions, UniFuse-Fusion [10] with ERP type images and cube maps, and light-weight UniFuse-Equi [10] with only ERP type images. As for the feature extractor of the ODI SR task, we directly employ the commonly-used EDSR-baseline [54] to extract features from the input LR ODIs. We down-sample ODIs with Bicubic interpolation, while down-sample omnidirectional depth maps with Nearest interpolation. During training, we augment data with horizontal flipping and rolling. We collaboratively train the two tasks for 30 epochs using the Adam optimizer [55] with batch size 2. The initial learning rate is set to $1e-4$, and reduced by 2 times per 5 epochs. For hyper-parameters in \mathcal{L}_{TOTAL} , we empirically set $\lambda_1 = \lambda_2 = 10$, and $\lambda_3 = \lambda_4 = \lambda_5 = 1$. For fair comparison, we re-train the compared methods based on their provided settings.

B. Quantitative and Qualitative Evaluation

We evaluate our method with standard metrics, including mean absolute error (MAE), absolute relative error (Abs Rel), root mean square error in log space (RMSE log). We also utilize three accuracy measures (δ_i), which are defined as the fraction of pixels where the relative error between

TABLE I
 QUANTITATIVE COMPARISON WITH FULLY-SUPERVISED METHODS (WITH HR DEPTH GT) ON STANFORD2D3D AND MATTERPORT3D DATASET.

Dataset	Backbone	Inp. size	Supervision	MAE ↓	Abs Rel ↓	RMSE log ↓	$\delta_1 \uparrow$	$\delta_2 \uparrow$	$\delta_3 \uparrow$
Stanford2D3D [29]	OmniDepth [14]	128×256 (×4)	Fully	0.3248	0.1653	0.1065	77.68	91.71	96.54
			Weakly (Ours)	0.3126	0.1566	0.1043	78.87	92.27	97.03
		64×128 (×8)	Fully	0.3484	0.1830	0.1117	75.71	90.90	96.13
			Weakly (Ours)	0.3480	0.1772	0.1154	75.85	90.59	96.19
	UniFuse-Fusion [10]	128×256 (×4)	Fully	0.2785	0.1409	0.0868	84.01	95.31	98.45
			Weakly (Ours)	0.2784	0.1398	0.0929	82.23	94.20	97.83
		64×128 (×8)	Fully	0.3124	0.1582	0.0975	80.16	93.03	97.46
			Weakly (Ours)	0.3135	0.1585	0.1037	78.06	92.71	97.37
	UniFuse-Equi [10]	128×256 (×4)	Fully	0.2732	0.1403	0.0870	83.70	94.90	98.24
			Weakly (Ours)	0.2747	0.1403	0.0908	83.13	94.83	98.25
		64×128 (×8)	Fully	0.3263	0.1619	0.1011	77.37	92.94	97.33
			Weakly (Ours)	0.3241	0.1630	0.1040	78.69	92.62	97.21
Matterport3D [30]	UniFuse-Fusion [10]	128×256 (×4)	Fully	0.3890	0.1547	0.0966	79.11	92.99	96.97
			Weakly (Ours)	0.3827	0.1569	0.0986	78.75	93.19	97.27
		64×128 (×8)	Fully	0.4779	0.1973	0.1179	70.90	88.98	95.29
			Weakly (Ours)	0.4767	0.2025	0.1220	69.80	89.21	95.57
		256×512 (×4)	Fully	0.3233	0.1314	0.0811	84.39	95.15	98.01
			Weakly (Ours)	0.3152	0.1264	0.0837	85.04	95.30	97.99
	OmniDepth [14]	128×256 (×4)	Fully	0.4483	0.1914	0.1127	72.95	90.21	95.75
			Weakly (Ours)	0.4237	0.1828	0.1082	74.44	91.34	96.51
		64×128 (×8)	Fully	0.4823	0.2127	0.1209	69.80	88.68	95.38
			Weakly (Ours)	0.4843	0.2076	0.1219	69.76	88.70	95.20

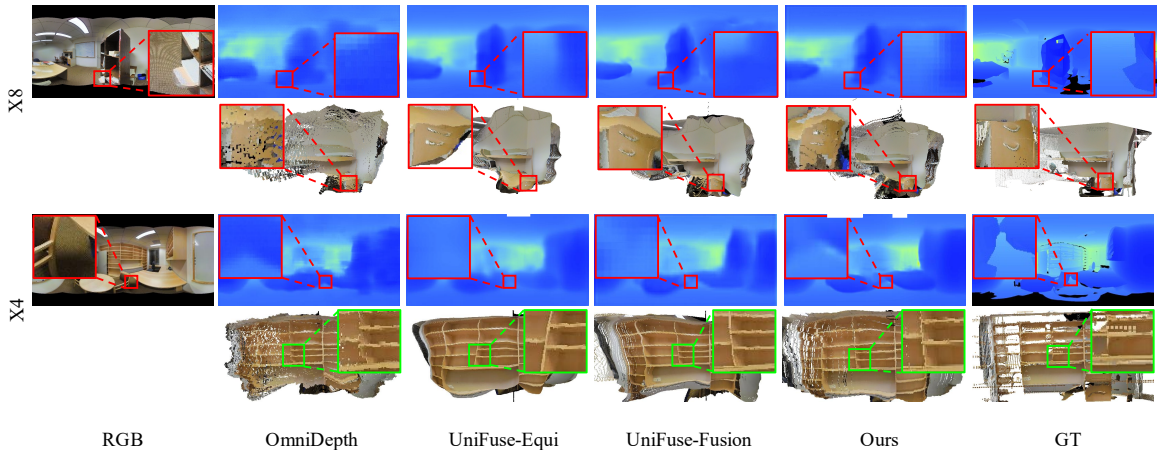


Fig. 4. Visual comparison of fully-supervised methods and ours on Stanford2D3D dataset. Best viewed in color.

the estimated depth and ground-truth depth is less than the threshold i , $i \in \{1.25, 1.25^2, 1.25^3\}$. We only measure on valid pixels in the ground-truth depth map.

Fully-supervised methods. We compare with fully-supervised methods that utilize HR depth GT maps. To the best of our knowledge, there are no existing methods designed to generate HR depth prediction from an LR ODI. To this end, we add learnable up-sampling convolutional layers to OmniDepth [14], UniFuse-Fusion [10], and UniFuse-Equi [10] and re-train them with HR depth GT maps. As shown in Tab. I, our weakly-supervised method not only achieves comparable results with corresponding fully-supervised methods (*e.g.*, 3rd-4th rows), but also outperforms corresponding supervised methods in some cases (*e.g.*, 1st-2nd rows). For example, in the 4th row of Fig. 4, our method predicts the bookshelf with regular shape, while the other corresponding fully-supervised

methods predict the shape with more or less warp.

The adaptability of our method in different input sizes is also verified, *e.g.*, 128×256 and 64×128 . Our weakly-supervised method outperforms the fully-supervised methods in several metrics, *e.g.*, MAE, Abs Rel, and δ_3 . For example, with OmniDepth as the backbone with 128×256 input size, our method obtains 3.8% gain in MAE metric and 5.3% gain in Abs Rel metric. When choosing a smaller input size 64×128 , our method can achieve similar results compared to the fully-supervised method, even though the LR depth GT map only contains 1/64 supervision signals of an HR depth GT map.

In addition, we train on Matterport3D dataset with UniFuse-Fusion and OmniDepth as backbone, and achieve comparable results with the corresponding fully-supervised methods. For example, with UniFuse-Fusion as backbone and $\times 8$ up-sampling factor, our method improves 1.6% in MAE met-

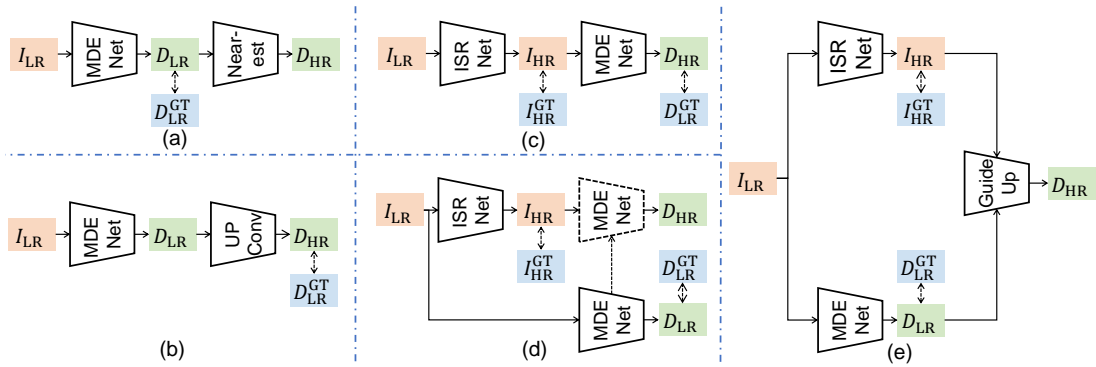


Fig. 5. The pipelines of baseline methods with five different settings. To be consistent with our weakly-supervised setting, these baseline methods only utilize LR ODIs as inputs and LR depth GT maps for supervision. MDE Net means the monocular depth estimation network, ISR Net means the ODI super-resolution network, Up Conv represents the learnable up-sampling convolutional layer, and Guide Up represents guided image filter [56].

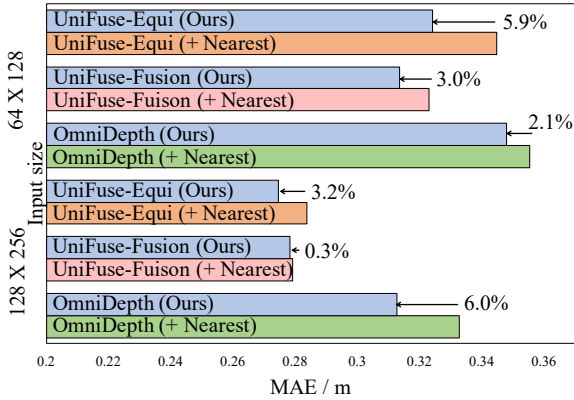


Fig. 6. Quantitative comparison with the baseline methods in the **Setting 1** with different up-sampling factors and backbones on Stanford2D3D dataset.

TABLE II
COMPARISON WITH THE BASELINE METHODS THAT USE LR ODIs AS INPUTS, AND LR DEPTH GROUND TRUTH MAPS FOR SUPERVISION.

	Abs Rel ↓	RMSE log ↓	δ_3 ↑
Setting 2	0.1830	0.1180	95.84
Setting 3	0.3848	0.2847	76.94
Setting 4	0.4523	0.3849	58.17
Setting 5	0.4422	0.2617	78.50
Ours	0.1585	0.1037	97.37

ric and 0.3% in δ_3 metric. Finally, in Tab. I, we verify the effectiveness of our method with higher resolution, *i.e.*, 1024×2048 . Given the input resolution is 256×512 and up-sampling factor is 4, the results show that our weakly-supervised method performs well. For example, compared with fully-supervised method, ours can improve 0.0050 in Abs Rel. **Baseline methods.** There are various ways to achieve HR omnidirectional depth estimation using an LR ODI as the input and an LR depth map for supervision. To fully verify the effectiveness of our framework, we compare our method with all possible baseline methods.

1) Setting 1: As shown in Fig. 5(a), it is to estimate LR depth map from LR input ODI, and directly up-sample the LR depth prediction with Nearest interpolation. As shown in Fig. 6, our method outperforms baseline methods with Nearest interpolation in different input sizes and backbones. For example, with OmniDepth as the backbone, our method

TABLE III
ABLATION STUDIES ON DIFFERENT SHARING STRATEGIES.

RGB (Mean)	Uncertainty (Variance)	Depth	MAE ↓	Abs Rel ↓
✓	—	✓	0.3225	0.1708
✓	—	✓	0.3179	0.1588
✓	✓	✓	0.3135	0.1585
✓	✓	✓	0.3234	0.1686

leads to 6.0% improvement in MAE metric, which proves the effects of structural knowledge transfer from the ODI SR task.

2) Setting 2: In Fig. 5(b), it is similar with Setting 1, except for replacing the Nearest interpolation with learnable up-sampling convolutional layers. The result of Setting 2 is 0.1830 Abs Rel metric, which is lower than our method (0.1585 Abs Rel). We analyze the reason is that the additional up-sampling convolutional layer can not be fully-supervised by HR depth GT maps, causing its performance dropped greatly.

3) Setting 3: In Fig. 5(c), it is to first up-sample LR ODIs with an ODI SR network, *i.e.*, EDSR-baseline [54], which is fully-supervised with HR ground truth ODIs. Then, the super-resolved ODI is fed into a depth estimation network to generate an HR depth prediction. The HR depth prediction is down-sampled with Nearest interpolation to be compared with the LR depth GT map. In Tab. II, the setting 3 performs badly, due to the super-resolved ODI contains much noise, which disturbs the following depth estimation network.

4) Setting 4: In Fig. 5(d), it is similar with Setting 3, except for that the depth estimation network is trained with LR ODI as input. We then directly transfer the pre-trained depth estimation network into the HR domain with the super-resolved ODI as input. However, it only obtains 0.4523 Abs Rel, which is worse than Setting 3 and our method. Its main drawback is that during training, the depth estimation network has no access to HR ODIs or HR depth maps.

5) Setting 5: In Fig. 5(e), it first predicts a super-resolved image with an ODI SR network, *i.e.*, EDSR-baseline [54], and an LR depth prediction with a depth estimation network. Then, it utilizes the super-resolved ODI to guide the interpolation process of the LR depth prediction with guided image filter [56] to obtain an HR depth prediction. However, the result is similar with that of Setting 4, due to the noise contained in the super-resolved image.

TABLE IV
ABLATION STUDIES ON CIIF ABOUT WHETHER LEARNING INTERPOLATION WEIGHTS, PARAMETER UPDATE, AND THE TYPE OF COORDINATE SYSTEM.

	Update	Coordinate	MAE ↓	Abs Rel ↓	δ_1 ↑
Bicubic	-	-	0.3209	0.1626	77.92
LIIF	Synchronous	Spherical	0.3302	0.1690	76.36
CIIF	Asynchronous	Cylindrical	0.3329	0.1692	76.94
CIIF	Synchronous	Cylindrical	0.3135	0.1585	78.06

C. Ablation Studies

All the experiments are done on Stanford2D3D dataset with $\times 8$ up-sampling factor.

Uncertainty estimation. In the first row of Tab. III, we first omit uncertainty estimation in the ODI SR task, and share the parameters of CIIF between feature up-sampling processes in the ODI SR task and HR depth estimation task. Removing uncertainty estimation leads to 2.8% MAE and 7.2% Abs Rel reduction. Directly transferring knowledge between the ODI SR task and HR depth estimation task obtains sub-optimal performance, because the redundant textural details in the ODI SR task might interfere with the HR depth estimation task.

Sharing strategy of CIIF. To verify the effectiveness of our proposed sharing strategy, we additionally experiment on other combinations in Tab. III. Specifically, in the second row, we choose to share the parameters of CIIF between feature up-sampling processes in the RGB part of the ODI SR task, and the HR depth estimation task. Moreover, we study the influence of sharing the parameters among the feature up-sampling processes in the RGB part of ODI SR task, the uncertainty part of ODI SR task, and the HR depth estimation task. However, we find that Abs Rel degrades 6.0% compared with sharing between the uncertainty part and HR depth estimation task. It also proves that textural details of directly transferring knowledge from features in the RGB part of ODI SR task can cause negative effects to the structural knowledge learning of the HR depth estimation task.

Components of CIIF. We replace CIIF with Bicubic interpolation followed by a convolution layer, which is commonly used in [10], [13]. In Tab. IV, we find that CIIF gains 2.5% in Abs Rel. We ascribe it as learning correlation among adjacent pixels is more effective for structural knowledge learning and transferring between different modals.

The parameters of CIIF are all contained in an MLP. We share the parameters of CIIF between the ODI SR task and HR depth estimation task. To verify it, we conduct a momentum update [52] for the HR depth estimation task, which is considered as a asynchronous update. From Tab. IV, asynchronous update reduces performance greatly. We think the reason is that scene structural knowledge is essential for the HR depth estimation task, and asynchronous update destroys the common structural representations between the two tasks.

In addition, we investigate the effectiveness of cylindrical representation. As shown in Tab. IV, exploiting cylindrical representation obtains 5.1% gain in MAE metric compared with utilizing spherical angle coordinates. Note that using spherical angle coordinates is equal to using planar pixel coordinates in LIIF [8], [44]. The result demonstrates that

TABLE V
ABLATION STUDIES ON LOSS FUNCTIONS.

\mathcal{L}_{LD}	\mathcal{L}_{FD}	Transform	Abs Rel ↓	δ_3 ↑
	✓	✓	0.1642	97.30
✓			0.1655	97.10
✓	✓		0.1723	97.34
✓	✓	✓	0.1585	97.37

TABLE VI
DISCUSSION ABOUT EMPLOYING DIFFERENT BACKBONES FOR THE ODI SR TASK.

	Abs Rel ↓	δ_3 ↑
SwinIR [57]	0.1673	96.99
Omni-SR [58]	0.1733	96.86
EDSR-baseline [54]	0.1585	97.37

TABLE VII
COMPARISON OF GENERALIZATION CAPABILITY.

	Method	MAE ↓	δ_3 ↑
Stanford2D3D →3D60	UniFuse-Fusion [10]	0.4816	94.51
	Ours	0.4637	95.02
Matterport3D →3D60	UniFuse-Fusion [10]	0.3974	96.88
	Ours	0.3629	97.05
Stanford2D3D →3D60	OmniDepth [14]	0.9735	71.07
	Ours	0.7761	81.47
Matterport3D →3D60	OmniDepth [14]	0.4363	95.29
	Ours	0.4250	95.95

cylindrical coordinate system is more proper to describe the spatial correlation of neighboring pixels in ERP type ODIs.

Loss function. By default, \mathcal{L}_{UISR} and \mathcal{L}_{HD} are necessary for the training. Therefore, we investigate the effectiveness of \mathcal{L}_{LD} and \mathcal{L}_{FD} . In Tab. V, without \mathcal{L}_{LD} , the performance degrades 3.5% in Abs Rel metric. It demonstrates that \mathcal{L}_{LD} can utilize the LR depth GT maps to help obtain more accurate LR features for the HR depth estimation task. Without \mathcal{L}_{FD} , the performance also degrades 1.6% in RMSE log metric. In addition, we directly measure the similarity between the features in the ODI SR task without transform and features in the HR depth estimation task, and find that Abs Rel metric degrades from 0.1585 to 0.1723.

D. Discussion

Different ODI SR backbones. In Tab. VI, we compare the performance with different backbones in the ODI SR task. *i.e.*, SwinIR, Omni-SR, and EDSR-baseline. However, we find that by employing deeper SR backbones, the performance of depth estimation drops. For example, with SwinIR as backbone, the Abs Rel metric drops 0.0088 compared with using EDSR-baseline. We think the reason is that the deeper SR backbones are not easy to train. Specifically, the Stanford2D3D dataset only contains 1000 training samples, which is not friendly for attention-based backbones. In addition, the deeper attention-based backbones need more time to converge. Instead, our employed depth estimation backbone, *e.g.*, OmniDepth, would converge in advance in the training process.

Generalization ability. To verify the generalization ability, we further test on 3D60 dataset with pre-trained depth es-

timization models, *i.e.*, OmniDepth and UniFuse-Fusion, from Stanford2D3D and Matterport3D datasets in Tab. VII. With UniFuse-Fusion as backbone, our weakly-supervised method outperforms the corresponding fully-supervised method, *e.g.*, 3.7% gain and 8.7% gain in MAE metric on Stanford2D3D dataset and Matterport3D dataset, respectively. With OmniDepth as backbone, our method also shows significant improvements, *e.g.*, 10.40% and 0.66% in δ_3 metric on Stanford2D3D and Matterport3D datasets, respectively.

V. CONCLUSION

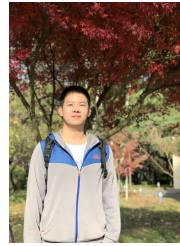
In this paper, to the best of our knowledge, we proposed the first work to estimate the HR omnidirectional depth map directly from an LR ODI, when no HR depth GT map is available. We found that the ODIs and their corresponding depth maps share the common scene structural knowledge. Therefore, we introduced an ODI SR task to boost the performance of the HR depth estimation task. Especially, the textural details in the ODI SR task can interfere with the smoothness of depth predictions. In this case, we introduced uncertainty estimation to the ODI SR specially for extracting scene structural knowledge. Upon this, we proposed the CIIF and FD loss in the SSKT module. The CIIF captures the correlations among neighboring pixels and shares the scene structural knowledge between the two tasks, while the FD loss provides extra structural regularization. Experimental results demonstrated that our weakly-supervised method is 1) efficient without extra inference cost, 2) flexible as a plug-and-play approach, and 3) effective to achieve comparable results with the fully-supervised methods.

Limitation and future work: In this paper, the feature up-sampling process in the HR depth estimation task is conducted with integral factors. In practice, predicting the depth maps with arbitrary resolution is required for practical usage. In the future, we will continue to explore how to predict HR omnidirectional depth map with arbitrary resolution from an LR ODI input, using LR depth maps for supervision.

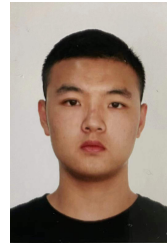
REFERENCES

- [1] E. Galván and P. Mooney, "Neuroevolution in deep neural networks: Current trends and future challenges," *IEEE Transactions on Artificial Intelligence*, vol. 2, no. 6, pp. 476–493, 2021.
- [2] D. Eigen, C. Puhrsch, and R. Fergus, "Depth map prediction from a single image using a multi-scale deep network," in *NIPS*, 2014.
- [3] L. Huynh, P. Nguyen-Ha, J. Matas, E. Rahtu, and J. Heikkilä, "Guiding monocular depth estimation using depth-attention volume," *ArXiv*, vol. abs/2004.02760, 2020.
- [4] J. Hu, M. Ozay, Y. Zhang, and T. Okatani, "Revisiting single image depth estimation: Toward higher resolution maps with accurate object boundaries," *2019 IEEE Winter Conference on Applications of Computer Vision (WACV)*, pp. 1043–1051, 2019.
- [5] J. H. Lee, M.-K. Han, D. W. Ko, and I. H. Suh, "From big to small: Multi-scale local planar guidance for monocular depth estimation," *ArXiv*, vol. abs/1907.10326, 2019.
- [6] I. Alhashim and P. Wonka, "High quality monocular depth estimation via transfer learning," *ArXiv*, vol. abs/1812.11941, 2018.
- [7] M. Mancini, G. Costante, P. Valigi, and T. A. Ciarfuglia, "Fast robust monocular depth estimation for obstacle detection with fully convolutional networks," *2016 IEEE/RSJ International Conference on Intelligent Robots and Systems (IROS)*, pp. 4296–4303, 2016.
- [8] H. Ai, Z. Cao, J. Zhu, H. Bai, Y. Chen, and L. Wang, "Deep learning for omnidirectional vision: A survey and new perspectives," *arXiv preprint arXiv:2205.10468*, 2022.
- [9] C. Sun, M. Sun, and H.-T. Chen, "Hohonet: 360 indoor holistic understanding with latent horizontal features," in *Proceedings of the IEEE/CVF Conference on Computer Vision and Pattern Recognition*, 2021, pp. 2573–2582.
- [10] H. Jiang, Z. Sheng, S. Zhu, Z. Dong, and R. Huang, "Unifuse: Uni-directional fusion for 360° panorama depth estimation," *IEEE Robotics and Automation Letters*, vol. 6, pp. 1519–1526, 2021.
- [11] H. Ai, Z. Cao, Y. pei Cao, Y. Shan, and L. Wang, "Hrdfuse: Monocular 360° depth estimation by collaboratively learning holistic-with-regional depth distributions," *ArXiv*, vol. abs/2303.11616, 2023.
- [12] F.-E. Wang, Y. hsuan Yeh, M. Sun, W.-C. Chiu, and Y.-H. Tsai, "Bifuse: Monocular 360 depth estimation via bi-projection fusion," *2020 IEEE/CVF Conference on Computer Vision and Pattern Recognition (CVPR)*, pp. 459–468, 2020.
- [13] Y. Li, Y. Guo, Z. Yan, X. Huang, Y. Duan, and L. Ren, "Omnifusion: 360 monocular depth estimation via geometry-aware fusion," in *Proceedings of the IEEE/CVF Conference on Computer Vision and Pattern Recognition*, 2022, pp. 2801–2810.
- [14] N. Zioulis, A. Karakottas, D. Zarpalas, and P. Daras, "Omniddepth: Dense depth estimation for indoors spherical panoramas," in *ECCV*, 2018.
- [15] M. Rey-Area, M. Yuan, and C. Richardt, "360monodepth: High-resolution 360° monocular depth estimation," *2022 IEEE/CVF Conference on Computer Vision and Pattern Recognition (CVPR)*, pp. 3752–3762, 2022.
- [16] K. Tateno, N. Navab, and F. Tombari, "Distortion-aware convolutional filters for dense prediction in panoramic images," in *ECCV*, 2018.
- [17] C. Zhuang, Z. Lu, Y. Wang, J. Xiao, and Y. Wang, "Acndnet: Adaptively combined dilated convolution for monocular panorama depth estimation," *arXiv preprint arXiv:2112.14440*, 2021.
- [18] C.-H. Peng and J. Zhang, "High-resolution depth estimation for 360deg panoramas through perspective and panoramic depth images registration," in *Proceedings of the IEEE/CVF Winter Conference on Applications of Computer Vision*, 2023, pp. 3116–3125.
- [19] S. Mangiante, G. Klas, A. Navon, Z. GuanHua, J. Ran, and M. D. Silva, "Vr is on the edge: How to deliver 360 videos in mobile networks," in *Proceedings of the Workshop on Virtual Reality and Augmented Reality Network*, 2017, pp. 30–35.
- [20] Z. Luo, B. Chai, Z. Wang, M. Hu, and D. Wu, "Masked360: Enabling robust 360-degree video streaming with ultra low bandwidth consumption," *IEEE Transactions on Visualization and Computer Graphics*, vol. 29, no. 5, pp. 2690–2699, 2023.
- [21] B. Sun, X. Ye, B. Li, H. Li, Z. Wang, and R. Xu, "Learning scene structure guidance via cross-task knowledge transfer for single depth super-resolution," *2021 IEEE/CVF Conference on Computer Vision and Pattern Recognition (CVPR)*, pp. 7788–7797, 2021.
- [22] A. Geiger, P. Lenz, and R. Urtasun, "Are we ready for autonomous driving? the kitti vision benchmark suite," in *2012 IEEE conference on computer vision and pattern recognition*. IEEE, 2012, pp. 3354–3361.
- [23] Y. Li and J. Ibanez-Guzman, "Lidar for autonomous driving: The principles, challenges, and trends for automotive lidar and perception systems," *IEEE Signal Processing Magazine*, vol. 37, no. 4, pp. 50–61, 2020.
- [24] X. Deng, H. Wang, M. Xu, Y. Guo, Y. Song, and L. Yang, "Lau-net: Latitude adaptive upscaling network for omnidirectional image super-resolution," *2021 IEEE/CVF Conference on Computer Vision and Pattern Recognition (CVPR)*, pp. 9185–9194, 2021.
- [25] Y.-S. Yoon, I. Chung, L. Wang, and K.-J. Yoon, "Spheresr: 360° image super-resolution with arbitrary projection via continuous spherical image representation," *ArXiv*, vol. abs/2112.06536, 2021.
- [26] X. Liu, D. Zhai, R. Chen, X. Ji, D. Zhao, and W. Gao, "Depth super-resolution via joint color-guided internal and external regularizations," *IEEE Transactions on Image Processing*, vol. 28, no. 4, pp. 1636–1645, 2018.
- [27] K. Karsch, C. Liu, and S. B. Kang, "Depth transfer: Depth extraction from video using non-parametric sampling," *IEEE transactions on pattern analysis and machine intelligence*, vol. 36, no. 11, pp. 2144–2158, 2014.
- [28] Q. Ning, W. Dong, X. Li, J. Wu, and G. Shi, "Uncertainty-driven loss for single image super-resolution," *Advances in Neural Information Processing Systems*, vol. 34, 2021.
- [29] I. Armeni, S. Sax, A. R. Zamir, and S. Savarese, "Joint 2d-3d-semantic data for indoor scene understanding," *ArXiv*, vol. abs/1702.01105, 2017.
- [30] A. Chang, A. Dai, T. Funkhouser, M. Halber, M. Niessner, M. Savva, S. Song, A. Zeng, and Y. Zhang, "Matterport3d: Learning from rgb-d data in indoor environments," *arXiv preprint arXiv:1709.06158*, 2017.

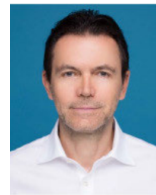
- [31] Z. Shen, C. Lin, K. Liao, L. Nie, Z. Zheng, and Y. Zhao, "Panoformer: Panorama transformer for indoor 360 depth estimation," *arXiv e-prints*, pp. arXiv-2203, 2022.
- [32] M. Li, S. Wang, W. Yuan, W. Shen, Z. Sheng, and Z. Dong, "S2net: Accurate panorama depth estimation on spherical surface," *IEEE Robotics and Automation Letters*, vol. 8, no. 2, pp. 1053–1060, 2023.
- [33] Z. Arican and P. Frossard, "Joint registration and super-resolution with omnidirectional images," *IEEE Transactions on Image Processing*, vol. 20, pp. 3151–3162, 2011.
- [34] L. Bagnato, Y. Boursier, P. Frossard, and P. Vanderghenst, "Plenoptic based super-resolution for omnidirectional image sequences," *2010 IEEE International Conference on Image Processing*, pp. 2829–2832, 2010.
- [35] H. Nagahara, Y. Yagi, and M. Yachida, "Super-resolution from an omnidirectional image sequence," *2000 26th Annual Conference of the IEEE Industrial Electronics Society. IECON 2000. 2000 IEEE International Conference on Industrial Electronics, Control and Instrumentation. 21st Century Technologies*, vol. 4, pp. 2559–2564 vol.4, 2000.
- [36] C. Ozcinar, A. Rana, and A. Smolic, "Super-resolution of omnidirectional images using adversarial learning," *2019 IEEE 21st International Workshop on Multimedia Signal Processing (MMSP)*, pp. 1–6, 2019.
- [37] F. Yu, X. Wang, M. Cao, G. Li, Y. Shan, and C. Dong, "Osr: Omnidirectional image super-resolution with distortion-aware transformer," in *Proceedings of the IEEE/CVF Conference on Computer Vision and Pattern Recognition*, 2023, pp. 13 283–13 292.
- [38] X. Sun, W. Li, Z. Zhang, Q. Ma, X. Sheng, M. Cheng, H. Ma, S. Zhao, J. Zhang, J. Li *et al.*, "Opdn: Omnidirectional position-aware deformable network for omnidirectional image super-resolution," in *Proceedings of the IEEE/CVF Conference on Computer Vision and Pattern Recognition*, 2023, pp. 1293–1301.
- [39] K.-S. Chung and C. Lee, "Gram: Gradient rescaling attention model for data uncertainty estimation in single image super resolution," *2019 18th IEEE International Conference On Machine Learning And Applications (ICMLA)*, pp. 8–13, 2019.
- [40] M. A. T. Figueiredo, "Adaptive sparseness using jeffreys prior," in *NIPS*, 2001.
- [41] L. Mescheder, M. Oechsle, M. Niemeyer, S. Nowozin, and A. Geiger, "Occupancy networks: Learning 3d reconstruction in function space," in *Proceedings of the IEEE/CVF conference on computer vision and pattern recognition*, 2019, pp. 4460–4470.
- [42] B. Mildenhall, P. P. Srinivasan, M. Tancik, J. T. Barron, R. Ramamoorthi, and R. Ng, "Nerf: Representing scenes as neural radiance fields for view synthesis," *Communications of the ACM*, vol. 65, no. 1, pp. 99–106, 2021.
- [43] S. Saito, T. Simon, J. Saragih, and H. Joo, "Pifuhd: Multi-level pixel-aligned implicit function for high-resolution 3d human digitization," in *Proceedings of the IEEE/CVF Conference on Computer Vision and Pattern Recognition*, 2020, pp. 84–93.
- [44] Y. Chen, S. Liu, and X. Wang, "Learning continuous image representation with local implicit image function," in *Proceedings of the IEEE/CVF conference on computer vision and pattern recognition*, 2021, pp. 8628–8638.
- [45] J. Tang, X. Chen, and G. Zeng, "Joint implicit image function for guided depth super-resolution," in *Proceedings of the 29th ACM International Conference on Multimedia*, 2021, pp. 4390–4399.
- [46] S. Niu, Y. Liu, J. Wang, and H. Song, "A decade survey of transfer learning (2010–2020)," *IEEE Transactions on Artificial Intelligence*, vol. 1, no. 2, pp. 151–166, 2020.
- [47] A. Mousavian, H. Pirsiavash, and J. Kosecka, "Joint semantic segmentation and depth estimation with deep convolutional networks," *2016 Fourth International Conference on 3D Vision (3DV)*, pp. 611–619, 2016.
- [48] Z. Liu, X. Qi, and C.-W. Fu, "3d-to-2d distillation for indoor scene parsing," *2021 IEEE/CVF Conference on Computer Vision and Pattern Recognition (CVPR)*, pp. 4462–4472, 2021.
- [49] L. xilinx Wang, D. Li, Y. Zhu, L. Tian, and Y. Shan, "Dual super-resolution learning for semantic segmentation," *2020 IEEE/CVF Conference on Computer Vision and Pattern Recognition (CVPR)*, pp. 3773–3782, 2020.
- [50] Y. Yang, Q. Cao, J. Zhang, and D. Tao, "Codon: On orchestrating cross-domain attentions for depth super-resolution," *International Journal of Computer Vision*, pp. 1–18, 2022.
- [51] D.-A. Clevert, T. Unterthiner, and S. Hochreiter, "Fast and accurate deep network learning by exponential linear units (elus)," *arXiv: Learning*, 2015.
- [52] K. He, H. Fan, Y. Wu, S. Xie, and R. Girshick, "Momentum contrast for unsupervised visual representation learning," in *Proceedings of the IEEE/CVF conference on computer vision and pattern recognition*, 2020, pp. 9729–9738.
- [53] I. Laina, C. Rupprecht, V. Belagiannis, F. Tombari, and N. Navab, "Deeper depth prediction with fully convolutional residual networks," in *2016 Fourth international conference on 3D vision (3DV)*. IEEE, 2016, pp. 239–248.
- [54] B. Lim, S. Son, H. Kim, S. Nah, and K. Mu Lee, "Enhanced deep residual networks for single image super-resolution," in *Proceedings of the IEEE conference on computer vision and pattern recognition workshops*, 2017, pp. 136–144.
- [55] D. P. Kingma and J. Ba, "Adam: A method for stochastic optimization," *arXiv preprint arXiv:1412.6980*, 2014.
- [56] K. He, J. Sun, and X. Tang, "Guided image filtering," *IEEE transactions on pattern analysis and machine intelligence*, vol. 35, no. 6, pp. 1397–1409, 2012.
- [57] J. Liang, J. Cao, G. Sun, K. Zhang, L. Van Gool, and R. Timofte, "Swinir: Image restoration using swin transformer," in *Proceedings of the IEEE/CVF international conference on computer vision*, 2021, pp. 1833–1844.
- [58] H. Wang, X. Chen, B. Ni, Y. Liu, and J. Liu, "Omni aggregation networks for lightweight image super-resolution," in *Proceedings of the IEEE/CVF Conference on Computer Vision and Pattern Recognition*, 2023, pp. 22 378–22 387.



Zidong Cao is a research assistant in the Visual Learning and Intelligent Systems Lab, Artificial Intelligence Thrust, Guangzhou Campus, The Hong Kong University of Science and Technology (HKUST). His research interests include 3D vision (depth completion, depth estimation, etc.), DL (self-supervised learning, weakly-supervised learning, etc.) and omnidirectional vision.



Hao Ai is a Ph.D. student in the Visual Learning and Intelligent Systems Lab, Artificial Intelligence Thrust, Guangzhou Campus, The Hong Kong University of Science and Technology (HKUST). His research interests include pattern recognition (image classification, face recognition, etc.), DL (especially uncertainty learning, attention, transfer learning, semi-/self-unsupervised learning), omnidirectional vision.



Athanasios V. Vasilakos is with the Center for AI Research (CAIR), University of Agder (UiA), Grimstad, Norway. He served or is serving as an Editor for many technical journals, such as the *IEEE TRANSACTIONS ON AI*, *IEEE TRANSACTIONS ON NETWORK AND SERVICE MANAGEMENT*, *IEEE TRANSACTIONS ON CLOUD COMPUTING*, *IEEE TRANSACTIONS ON INFORMATION FORENSICS AND SECURITY*, *IEEE TRANSACTIONS ON CYBERNETICS*; *IEEE TRANSACTIONS ON NANOBIOSCIENCE*; *IEEE TRANSACTIONS ON INFORMATION TECHNOLOGY IN BIOMEDICINE*; *ACM Transactions on Autonomous and Adaptive Systems*; the *IEEE JOURNAL ON SELECTED AREAS IN COMMUNICATIONS*. He is WoS highly cited researcher(HC).



Lin Wang (IEEE Member) is an assistant professor in the AI Thrust, CMA Trust at HKUST, GZ, and an affiliate assistant professor in the Dept. of CSE, HKUST, CWB. He did his Postdoc at the Korea Advanced Institute of Science and Technology (KAIST). He got his Ph.D. (with highest honors) and M.S. from KAIST, Korea. He had rich cross-disciplinary research experience, covering mechanical, industrial, and computer engineering. His research interests lie in computer and robotic vision, machine learning, intelligent systems (XR, vision for HCI), etc. For more about me, please visit <https://vllislab22.github.io/vllislab/>.